

# One-Step Synthesis and Optical and Electrical Properties of Thin Film $\text{Cu}_3\text{BiS}_3$ for Use as a Solar Absorber in Photovoltaic Devices

Nathan J. Gerein and Joel A. Haber\*

Department of Chemistry, University of Alberta, Edmonton, Alberta, T6G 2G2 Canada

Received June 22, 2006. Revised Manuscript Received October 10, 2006

We have synthesized  $\text{Cu}_3\text{BiS}_3$  thin films on fused silica substrates in a one-step process by reactive sputter deposition of Cu–S and Bi on hot substrates. This one-step process produces films that are crystalline, phase-pure, dense, smooth, and continuous. As-deposited films have a direct forbidden band gap of 1.4 eV, an optical absorption coefficient of  $1 \times 10^5 \text{ cm}^{-1}$  at 1.9 eV, p-type conductivity, and an electrical resistivity of  $84 \text{ } \Omega\cdot\text{cm}$ . Postdeposition annealing in an  $\text{H}_2\text{S}$  atmosphere increases crystallite size and reduces electrical resistivity of films to  $9.6 \text{ } \Omega \text{ cm}$ .

## Introduction

Semiconductor thin films with a band gap of 0.9–1.9 eV are suitable for use as the solar absorber layer in thin film photovoltaic devices. Currently, the technologically relevant semiconductors for thin film photovoltaic applications are  $\text{Cu}(\text{In,Ga})\text{Se}_2$  (CIGS) and  $\text{CdTe}$ , with devices based on each material having reached commercialization. However, it has been reported that the availability of tellurium and indium may limit the generating capacity of these devices to 4% of current global electricity demand for  $\text{CdTe}$  and 1% for CIGS.<sup>1</sup> As a consequence, the development of new semiconductors for use in thin film photovoltaics is required if these devices are to play a significant long-term role in global energy production. A promising source of alternative materials to CIGS and  $\text{CdTe}$  is the large number of known sulfide minerals, some of which are expected to have suitable optical and electrical properties for photovoltaic applications.<sup>2</sup>

The sulfide mineral Wittichenite,  $\text{Cu}_3\text{BiS}_3$ , has been synthesized in thin film form by other researchers using the solid-state reaction of chemical-bath-deposited  $\text{CuS}$  and thermally evaporated Bi films.<sup>3</sup> Optical and electrical properties of the resulting  $\text{Cu}_3\text{BiS}_3$  thin films suggest that it meets the basic requirements for use as a solar absorber in photovoltaic devices.<sup>3</sup>  $\text{Cu}_3\text{BiS}_3$  is also compatible with the objective of minimizing concerns about material availability and toxicity. Bismuth is currently used in pharmaceuticals and as a replacement for lead in ammunition, solders, and other materials where toxicity is a concern.<sup>4</sup> Bismuth is readily available, and the use of bismuth-containing compounds in place of CIGS or  $\text{CdTe}$  would raise the energy

production ceiling of thin film photovoltaic technologies. The U.S. Geological Survey lists current global reserves of bismuth at 330 000 metric tons, whereas current global tellurium reserves are 21 000 metric tons and current global indium reserves are 2 500 metric tons.<sup>4</sup> Bismuth is easily obtained directly from a bismuth ore, although some bismuth mines are currently on stand-by because of lack of demand. As a result, bismuth is most commonly obtained as a byproduct during the refining of lead.<sup>4</sup>

It is our expectation that the development of physical vapor deposition synthetic methods for  $\text{Cu}_3\text{BiS}_3$ , as well as other potential solar absorber materials, will facilitate the introduction and utilization of these new materials in photovoltaic devices because of their compatibility with existing technologies and large-scale manufacturing. In a companion paper, we have reported a two-step synthesis for  $\text{Cu}_3\text{BiS}_3$  by heating metal and metal sulfide precursors in an  $\text{H}_2\text{S}$  atmosphere.<sup>5</sup> However,  $\text{Cu}_3\text{BiS}_3$  films synthesized by this two-step process contained voids and pockets between the film and substrate, even when optimized processing conditions were employed, making them unsuitable for use in thin film PVs.<sup>5</sup>

In this paper, we report a different approach for the synthesis of  $\text{Cu}_3\text{BiS}_3$ , utilizing sputter deposition directly onto hot substrates. Physical vapor deposition directly onto hot substrates under inert or reactive conditions has been utilized successfully for the synthesis of a wide variety of crystalline thin films, including  $\text{CuInS}_2$ ,<sup>6</sup>  $\text{Cu}_2\text{S}$ ,<sup>7</sup>  $\text{SnS}$ ,<sup>8</sup>  $\text{In}_2\text{O}_3$ ,<sup>9–11</sup>  $\text{CuO}$ ,<sup>12</sup>

\* Corresponding author. E-mail: joel.haber@ualberta.ca.

(1) Andersson, B. A. *Prog. Photovolt.* **2000**, *8*, 61–76.  
 (2) Dittrich, H.; Vaughan, D. J.; Patrick, R. A. D.; Graeser, S.; Lux-Steiner, M.; Kunst, R.; Lincot, D. In *Proceedings of the 13th European Photovoltaic Solar Energy Conference*, Nice, France, Oct 23–27, 1995; pp 1299–1302.  
 (3) Estrella, V.; Nair, M. T. S.; Nair, P. K. *Semicond. Sci. Technol.* **2003**, *18*, 190–194.  
 (4) George, M. W. *Mineral Commodity Summaries*; U.S. Geological Survey Report; U.S. Government Printing Office: Washington, DC, 2005.

(5) Gerein, N. J.; Haber, J. A. *Chem. Mater.* **2006**, *18*, 6289–6296.  
 (6) Ellmer, K.; Hinze, J.; Klaer, J. *Thin Solid Films* **2002**, *413*, 92–97.  
 (7) He, Y.; Kriegseis, W.; Bläsing, J.; Polity, A.; Krämer, T.; Hasselkamp, D.; Meyer, B. K.; Hardt, M.; Krost, A. *Jpn. J. Appl. Phys., Part 1* **2002**, *41*, 4630–4634.  
 (8) Reddy, N. K.; Ramesh, K.; Ganesan, R.; Reddy, K. T. R.; Gunasekhar, K. R.; Gopal, E. S. R. *Appl. Phys. A* **2006**, *83*, 133–138.  
 (9) Gopchandran, K. G.; Joseph, B.; Abraham, J. T.; Koshy, P.; Vaidyan, V. K. *Vacuum* **1997**, *48*, 547–550.  
 (10) Casey, V.; Stephenson, M. I. *J. Phys. D: Appl. Phys.* **1990**, *23*, 1212–1215.  
 (11) Amaral, A.; Brogueira, P.; Nunes de Carvalho, C.; Lavareda, G. *Surf. Coat. Technol.* **2000**, *125*, 151–156.  
 (12) Ghosh, S.; Avasthi, D. K.; Shah, P.; Ganesan, V.; Gupta, A.; Sarangi, D.; Bhattacharya, R.; Assmann, W. *Vacuum* **2000**, *57*, 377–385.

and  $\text{Zn}_{1-x}\text{Mg}_x\text{O}$ .<sup>13</sup> Our one-step reactive deposition for  $\text{Cu}_3\text{-BiS}_3$  yields thin films that are continuous and dense and have a smooth mirrorlike surface, the morphology appropriate for photovoltaic device applications. These as-deposited films are also crystalline and phase-pure and have the requisite optical and electrical properties for photovoltaic applications. Postdeposition annealing in an  $\text{H}_2\text{S}$  atmosphere increases crystallite size and decreases the resistivity of the film. Details on the synthesis, structure, morphology, and optical and electrical properties of these films, as well as the effect of postdeposition processing in an  $\text{H}_2\text{S}$  atmosphere, are reported herein.

### Experimental Section

Films were sputter deposited directly on fused silica substrates (50 mm  $\times$  50 mm). Substrates were cleaned in 2-propanol in an ultrasonic bath for 30 min, immersed for 30 min in a 1:3 mixture of  $\text{H}_2\text{O}_2\text{:H}_2\text{SO}_4$ , rinsed with distilled  $\text{H}_2\text{O}$ , rinsed with 2-propanol, and dried under  $\text{N}_2$ . During the deposition, substrates were maintained at temperatures of 250–300 °C. This temperature range was previously identified as optimal for synthesis of  $\text{Cu}_3\text{BiS}_3$  thin films.<sup>5,14</sup> Substrates were heated by quartz lamps, and the temperature was monitored by a thermocouple in contact with the substrate platen. During the deposition, the platen was continuously rotated at 6 rpm. Films were deposited by sputter deposition from a CuS target at 80 W RF and a Bi target at 10 W DC. Targets were 3 in. in diameter, and the sputtering gas was Ar at a pressure of 5 mTorr. Stoichiometry of single composition, multielement films deposited on unheated substrates was determined by wavelength dispersive X-ray spectroscopy (WDX). Cu–S films were found to be sulfur-poor relative to the target, with a composition of 2.8:1.0 Cu:S. When the CuS target was cosputtered with the Bi target, Cu–S–Bi films were sulfur-rich relative to the target, with a composition of 1.0:3.2:1.9 Cu:S:Bi.

To deposit compound films on hot substrates with the desired 3:1:3 stoichiometry, we sputtered the CuS target continuously and cycled the Bi target on and off. The correct elemental ratio was achieved by cosputtering CuS and Bi targets for 5 min, followed by CuS target sputtering for 25–30 min, depending on substrate temperature. Hotter substrates required shorter CuS-only sputter times to compensate for the increased sublimation of Bi. Each cycle produced approximately 75 nm of deposition and was repeated 4 or 8 times, resulting in films with final thicknesses of approximately 300 or 600 nm, respectively. Following deposition, the substrate temperature was maintained at the deposition temperature (250–300 °C) for 30 min, followed by cooling to 100 °C at 2 °C/minute. Some films were subsequently annealed at 250–300 °C for 2 h under 1 Torr  $\text{H}_2\text{S}/49$  Torr Ar, followed by cooling to 100 °C at 2 °C/minute. The volume of the annealing chamber is approximately 40 L, with heating provided by a programmable resistance heater.

Composition and morphology of the thin films were characterized using scanning electron microscopy/energy dispersive X-ray spectroscopy (SEM/EDX) (JEOL 6031F FESEM, Hitachi S-4800 FESEM), WDX (JEOL 8900 microprobe), and X-ray diffraction (XRD) (Bruker D8 diffractometer with area detector). Additional characterization was carried out to measure the optical and electrical properties of the thin films. Transmission and reflection data (Bruker

Vertex 70) was used to determine the optical band gap, band gap type, and optical absorption coefficient. For transmission measurements, a clean fused silica substrate was used as the 100% transmission standard. Reflection measurements were made at 10° from normal, and an aluminum mirror deposited on a fused silica substrate was used as the 100% reflection standard. Sheet and electrical resistivities were measured using a 4-point probe (Jandel 4-point probe with 0.5 mm probe spacing, Keithly 2400 Sourcemeter). Measurements were taken with a constant current set at 0.01–0.05  $\mu\text{A}$  to produce a voltage drop in the range of 2–4 mV. These conditions minimized carrier injection and produced stable and consistent measurements. Doping type was determined using hot probe measurements with a hot probe temperature of 50–60 °C (in-house manufactured probe, Fluke DMM).

### Results

Films of high quality were synthesized directly on fused silica substrates at temperatures of 250–300 °C; however, the morphology of the films varied over this temperature range, and changes in deposition parameters were required to compensate for the increased Bi vapor pressure at higher temperatures. We have previously reported that 300 °C is the maximum processing temperature for  $\text{Cu}_3\text{BiS}_3$ ,<sup>14</sup> with film decomposition and Bi sublimation occurring at higher temperatures. In the present work, increasing the substrate temperature from 250 to 300 °C is accompanied by an increase in Bi sublimation. To compensate for this, it is necessary to decrease the CuS-only sputter time from 30 to 25 min with a constant cosputtered period of 5 min. Consistent with our previous work, 300 °C is the maximum temperature at which this reactive deposition can be carried out successfully.

Changes in morphology as a function of substrate temperature were most evident when films were observed at a fracture. Films deposited at 300 °C were homogeneous throughout the depth of the film, whereas those deposited at 250 °C retained the layered structure of the deposition. SEM images of a film deposited at 300 °C are presented in images a and b of Figure 1. The film is smooth and continuous when viewed from the surface and dense and homogeneous when viewed edge-on at a fracture. SEM images a and b in Figure 2 for a  $\text{Cu}_3\text{BiS}_3$  film deposited at 250 °C show the film is smooth and continuous when viewed from the surface (Figure 2a). When viewed edge-on at a fracture, the film is observed to retain the layered structure of the deposition, with each of the 8 layers clearly visible (Figure 2b). For all films, backscattered SEM imaging was used to screen for secondary phases, with none detected, and the 3:1:3 Cu:Bi:S composition of the films was confirmed by EDX.

XRD powder patterns were used to identify the phase of all films. Films deposited at both 250 and 300 °C were identified as phase-pure and crystalline; however, differences in the intensity of the peaks were observed to correlate with deposition temperature. The powder pattern collected from a film deposited with a substrate temperature of 300 °C and the standard powder pattern for  $\text{Cu}_3\text{BiS}_3$  (PDF 43-1479) are shown in panels c and d of Figure 1, respectively. The amorphous hump centered at 22°  $2\theta$  is attributed to the fused silica substrate. Film texture is evident in the powder pattern, with enhanced intensity (relative to the standard powder

(13) Hwang, D.-K.; Jeong, M.-C.; Myoung, J.-M. *Appl. Surf. Sci.* **2004**, *225*, 217–222.

(14) Gerein, N. J.; Haber, J. A. In *Thin-Film Compound Semiconductor Photovoltaics*; Shafarman, W., Gessart, T., Niki, S., Siebentritt, S., Eds.; Material Research Society: Warrendale, PA, 2005; Vol. 865, pp F5.2.1–F5.2.6.

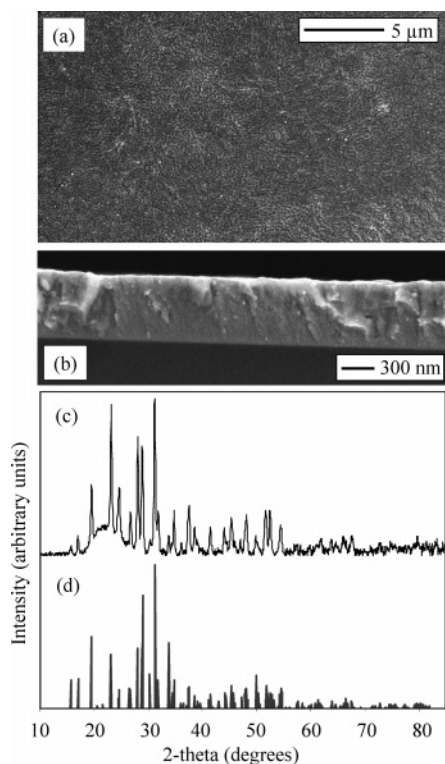


**Figure 1.** (a,b) SEM images of a  $\text{Cu}_3\text{BiS}_3$  film synthesized by reactive deposition with a substrate temperature of 300 °C, (c) powder pattern of the film, and (d) standard powder pattern for  $\text{Cu}_3\text{BiS}_3$ .

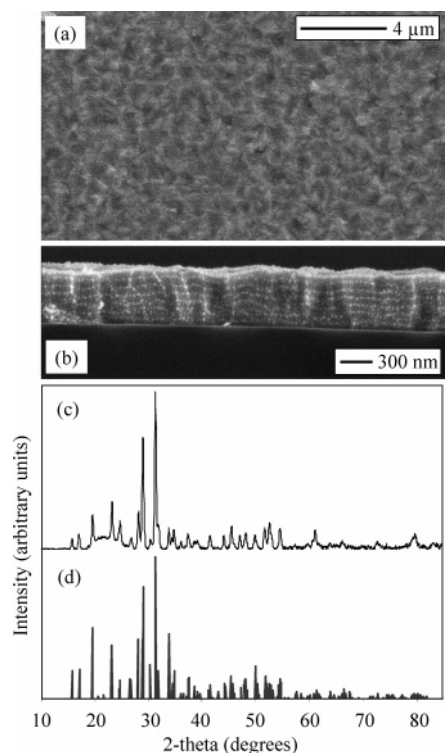


**Figure 2.** (a,b) SEM images of a  $\text{Cu}_3\text{BiS}_3$  film synthesized by reactive deposition with a substrate temperature of 250 °C, (c) powder pattern of the film, and (d) standard powder pattern for  $\text{Cu}_3\text{BiS}_3$ .

pattern) of the 200 and 211 peaks at 23.1 and 28.1°  $2\theta$ , respectively. The powder pattern collected from a film deposited with a substrate temperature of 250 °C and the standard powder pattern for  $\text{Cu}_3\text{BiS}_3$  are presented in c and d of Figure 2, respectively. As with the film deposited at

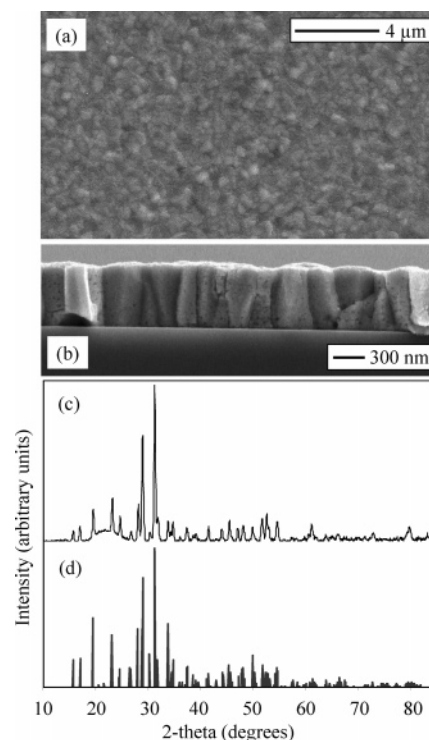


**Figure 3.** (a,b) SEM images of a  $\text{Cu}_3\text{BiS}_3$  film synthesized by reactive deposition with a substrate temperature of 250 °C (see Figure 2), followed by annealing at 300 °C under 1 Torr  $\text{H}_2\text{S}/49$  Torr Ar for 2 h, (c) powder pattern of the annealed film, and (d) standard powder pattern for  $\text{Cu}_3\text{BiS}_3$ .

higher temperature, the film is crystalline, with the amorphous hump at 22°  $2\theta$  attributed to the fused silica substrate. However, at the lower deposition temperature of 250 °C, the intensity profile of the experimental powder pattern is a good match with the standard powder pattern, indicating a random orientation of the crystallites.

Following reactive deposition, films were annealed under 1 Torr  $\text{H}_2\text{S}/49$  Torr Ar for 2 h at 250–300 °C to assess the effect on film properties. The most significant changes were observed when films deposited at 250 °C were annealed at 300 °C. Annealing at lower temperatures resulted in similar changes, but the effects were less pronounced. SEM images and the XRD powder pattern of a film deposited at 250 °C (Figure 2) and then annealed at 300 °C are presented in Figure 3. SEM images and the XRD powder pattern of a film deposited at 300 °C (Figure 1) and then annealed at 300 °C are presented in Figure 4. It should be noted that although significant morphological differences were observed between the as-deposited films, the annealed films are very similar in appearance. Most noteworthy is the fact that the layered structure of the film deposited at 250 °C is eliminated. The only morphological difference between the two films following annealing is the residual presence of very small voids (indicating lower density) in the film deposited at 250 °C relative to the film deposited at 300 °C. In both cases, postdeposition annealing increased the crystallite size, producing individual crystallites in the 0.5–1  $\mu\text{m}$  range. These larger crystallites are columnar in shape and generally extended the entire depth of the film. Crystal growth was accompanied by a slight increase in the roughness of the film; however, annealed films retained the mirrorlike surface of the as-deposited films. XRD powder

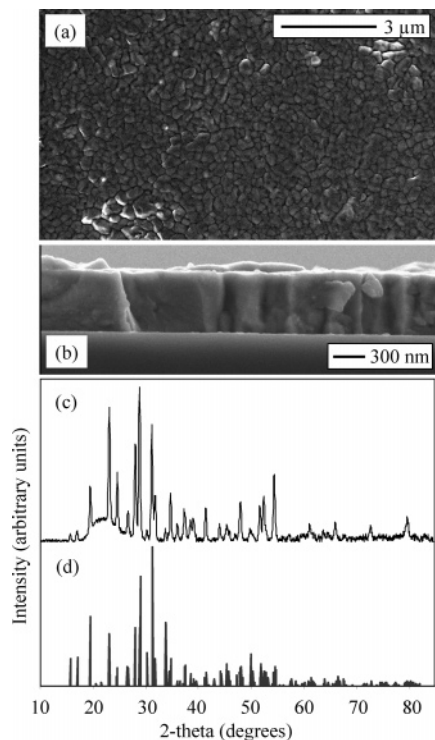


**Figure 4.** (a,b) SEM images of a  $\text{Cu}_3\text{BiS}_3$  film synthesized by reactive deposition with a substrate temperature of 300 °C, followed by annealing at 300 °C under 1 Torr  $\text{H}_2\text{S}/49$  Torr Ar for 2 h, (c) powder pattern of the annealed film, and (d) standard powder pattern for  $\text{Cu}_3\text{BiS}_3$ .

pattern data collected from the annealed films show that the random orientation of films deposited at 250 °C is retained in the annealed film, with no indication of texture. Similarly, films deposited at 300 °C retained the preferred orientation along the [200]/[211] directions following annealing.

Transmission and reflection data collected from a 300 nm thick, as-deposited film are presented in Figure 5a. Similar data was collected from both as-deposited and annealed films with a thickness of 600 nm. No changes in optical properties were observed, demonstrating that there is no dependence of band gap on film thickness. This data was used to determine the energy-dependent optical absorption coefficient and the nature and magnitude of the optical band gap. The optical absorption coefficient can be calculated from

$$\alpha = 1/x \ln[(1 - R)^2/T]$$

where  $x$  is the film thickness and  $R$  and  $T$  are reflection and transmission values, respectively.<sup>15</sup> Plotted in Figure 5b is  $\alpha$  as a function of energy, with  $\alpha = 1 \times 10^5 \text{ cm}^{-1}$  at 1.9 eV. The nature and magnitude of the optical band gap may be determined from the fact that  $\alpha h\nu$  is proportional to  $(h\nu - E_g)^n$ . As a consequence, plots of  $(\alpha h\nu)^{1/n}$  against  $h\nu$ , with  $1/n = 2, 2/3, 1/2, 1/3$ , for direct, direct forbidden, indirect, and indirect forbidden, respectively, are linear, with the intercept yielding the value of the band gap.<sup>15</sup> A plot of  $(\alpha h\nu)^{2/3}$  against  $h\nu$  is shown in Figure 5c; the linear plot identifies the band gap as direct forbidden, and the intercept gives the magnitude of the band gap as 1.4 eV. For comparison purposes, plots of  $(\alpha h\nu)^{1/n}$  against  $h\nu$  for all four

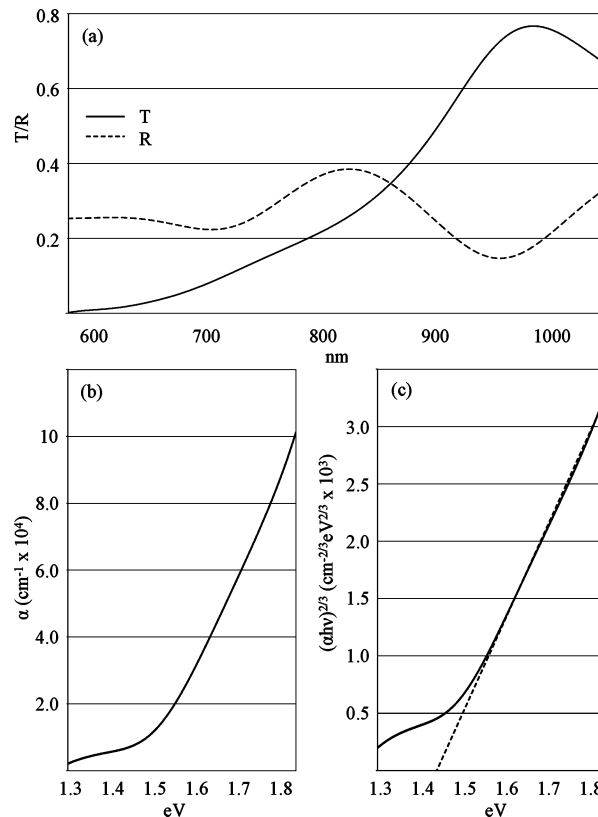


**Figure 5.** (a) Transmission (solid line) and reflection (dashed line) against wavelength collected from a 300 nm thick  $\text{Cu}_3\text{BiS}_3$  film, used to calculate (b)  $\alpha$  as a function of energy, and (c)  $(\alpha h\nu)^{2/3}$  as a function of energy with dashed line of best fit showing an  $x$ -intercept of 1.4 eV (direct forbidden optical band gap).

values of  $1/n$  are available in the Supporting Information (Figure S1).

The sheet and electrical resistivity of the films was measured using a 4-point probe<sup>16</sup> on both as-deposited and annealed films with a thickness of 600 nm. It was found that the sheet resistivity decreased by an order of magnitude from  $1.4 \times 10^6 \Omega$  to  $1.6 \times 10^5 \Omega$  when as-deposited films were annealed at 300 °C. The corresponding electrical resistivity values for these films are 84  $\Omega \text{ cm}$  and 9.6  $\Omega \text{ cm}$ , respectively. There was no significant variation in resistivity with deposition temperature. However, a slight increase in resistivity was observed in films aged in air for several weeks, presumably due to surface oxidation. Any oxidation that occurred was not detectable by XRD. Hot probe measurements were used to determine majority carrier type,<sup>16</sup> with all films clearly indicating p-type conductivity regardless of deposition temperature or postdeposition processing.

## Discussion

For thin film photovoltaics to play a significant role in global energy production, new materials will be required whose deployment is not limited by raw material availability. The development of successful devices incorporating new materials is likely to involve not only identifying new

(15) Pankove, J. I. *Optical Processes in Semiconductors*; Prentice Hall, Inc.: Englewood Cliffs, NJ, 1971.

(16) Schroder, D. K. Resistivity. In *Semiconductor Material and Device Characterization*, 2nd ed.; John Wiley and Sons, Inc.: New York, 1998; pp 2–17.

absorber materials, but other mutually compatible layers as well. This is a significant challenge and a critical first step is the development of simple, efficient syntheses for individual components. This paper reports a successful one-step deposition for high-quality  $\text{Cu}_3\text{BiS}_3$  thin films, with measured optical and electrical properties that support its potential application as an absorber layer in thin film PVs.

In a companion publication, we reported a two-step synthesis of phase-pure  $\text{Cu}_3\text{BiS}_3$  thin films by heating metal and metal sulfide precursor films in an  $\text{H}_2\text{S}$  atmosphere; however, for both precursor types, the reaction pathway was found to have a controlling influence on film morphology.<sup>5</sup> In the case of metal precursor films, the formation of a discontinuous  $\text{Cu}_{1.8}\text{S}$  intermediate followed by slow reaction with Bi translated into holes in the final film. In the case of metal sulfide precursors, volume expansion during the reaction of intermediate phases formed during sputter deposition resulted in buckling of the product film.<sup>5</sup> In the one-step synthesis detailed in this paper, the reactive deposition is critical to avoiding the fundamental limitations of the two-step process for the synthesis of  $\text{Cu}_3\text{BiS}_3$  thin films on fused silica substrates. The growth of  $\text{Cu}_3\text{BiS}_3$  films by the one-step method is thought to proceed as follows. During the initial, cosputtered period,  $\text{Cu}_3\text{BiS}_3$  is synthesized along with excess Bi. Previous results from depositions on unheated substrates show that the Bi reacts with Cu–S during cosputtering, producing  $\text{Bi}_2\text{S}_3$ . Therefore, excess Bi is expected to be primarily present as  $\text{Bi}_2\text{S}_3$ .<sup>5</sup> During the second phase of the cycle, only Cu–S is deposited, which reacts with the excess Bi or  $\text{Bi}_2\text{S}_3$  in the film, adding to the initially formed crystalline  $\text{Cu}_3\text{BiS}_3$ . This layered crystalline growth is supported by the observation of such a structure in the cross-section of films deposited at lower temperatures (Figure 2b). The success of this one-step deposition is also consistent with our previous results on the reactive annealing of metal sulfide precursor films. In each method, similar deposition techniques are employed; however, in the two-step process, buckling occurs during conversion of the precursor film to the product film and is attributed to the reaction of intermediate phases and additional sulfur uptake.<sup>5</sup> The one-step reactive deposition method enables us to avoid these pitfalls by the direct layer-by-layer buildup of the  $\text{Cu}_3\text{BiS}_3$  film without a sulfur deficiency.

This one-step deposition is attractive not only for its simplicity but also for the control it provides over the final film structure. Films formed at lower deposition temperatures contain small crystallites with a random orientation. Films deposited at higher temperatures have larger crystallites that exhibit a preferred orientation in the [200]/[211] directions. In each case, the crystallinity of the films may be improved by a postdeposition annealing that results in the formation of larger crystallites that span the thickness of the film and are orientated perpendicular to the substrate. Significantly, the random or preferred orientation of the crystallites in the as-deposited films is preserved during this postdeposition processing step, a subtlety that could prove useful for optimizing device performance if  $\text{Cu}_3\text{BiS}_3$  films are successfully incorporated into thin film PVs. Similar control over film texture has been achieved with CIGS thin films, with

films having random orientation or preferred orientation in the [112] or [220]/[204] directions all being employed in PV devices.<sup>17</sup> The orientation of the crystallites perpendicular to the substrate is also ideal for use in PV devices, because this is the direction of charge transport; this particular orientation would be expected to facilitate carrier movement through the bulk of the crystallites or along grain boundaries and surfaces.

The electrical properties of the  $\text{Cu}_3\text{BiS}_3$  thin films synthesized in this manner are also suitable for incorporation into conventional thin film devices, because both as-deposited and annealed films show p-type conductivity, a requirement for use with conventional n-type transparent conducting oxides and buffer layers. The electrical resistivity of as-deposited films is  $84 \text{ } \Omega \text{ cm}$ ; following annealing, this drops to  $9.6 \text{ } \Omega \text{ cm}$ . This is comparable to the previously reported value of  $30 \text{ } \Omega \text{ cm}$ .<sup>3</sup> The direct forbidden optical band gap of 1.4 eV is also close to the optimum for single-junction PV applications, and although the direct forbidden band gap results in a slower rise of the optical absorption coefficient, it reaches a value of  $1.0 \times 10^5 \text{ cm}^{-1}$  at 1.9 eV. These values are virtually identical with the previously reported direct forbidden optical band gap of 1.3 eV and optical absorption coefficient of  $1 \times 10^5 \text{ cm}^{-1}$  at 1.9 eV.<sup>3</sup> The similarity of the optical and electrical measurements we have reported to those previously reported by Nair and co-workers suggest that  $\text{Cu}_3\text{BiS}_3$  is amenable to a variety of synthetic strategies. This synthetic flexibility could prove useful by enabling a variety of approaches to the integration of  $\text{Cu}_3\text{BiS}_3$  into PV devices.

The high quality of the as-deposited films produced by the one-step deposition method we have reported, the improvements in film quality resulting from postdeposition annealing, and the measured optical and electrical properties all support the integration of  $\text{Cu}_3\text{BiS}_3$  thin films into PV devices. To better assess the suitability of these films for use as a solar absorber, we are currently performing more detailed characterization to determine a wider range of material properties, including carrier lifetime, concentration, and mobility, as well as the effect of processing variations on these properties. We are also actively pursuing the development of preliminary devices using PVD techniques and have previously reported a combinatorial strategy we plan to implement to realize rapid device optimization on the basis of  $\text{Cu}_3\text{BiS}_3$  or other promising novel absorber materials.<sup>14</sup> A key first step in device development has been achieved by the successful application of our one-step reactive deposition method to the synthesis of  $\text{Cu}_3\text{BiS}_3$  thin films on indium tin oxide (ITO)-coated soda-lime glass substrates.<sup>18</sup>

## Conclusions

We have developed a one-step reactive deposition for the synthesis of  $\text{Cu}_3\text{BiS}_3$  thin films. This process is appealing because of its simplicity as well as its compatibility with

(17) Kemell, M.; Ritala, M.; Leskelä, M. *Crit. Rev. Solid State Mater. Sci.* **2005**, *30*, 1–31.

(18) Gerein, N. J.; Haber, J. A. In *Proceedings of the IEEE 4th World Conference on Photovoltaic Energy Conversion*, Waikoloa, HI, May 7–12, 2006; in press.

PVD techniques that are widely employed in the production of thin film devices. As-deposited  $\text{Cu}_3\text{BiS}_3$  films are crystalline, smooth, continuous, and phase-pure. The crystallite size of these films may be increased and resistivity decreased by a subsequent annealing process, while maintaining the smooth, continuous aspects of the as-deposited films. The morphology of the films is ideal for incorporation into thin film photovoltaic devices. Optical and electrical properties of the films, including a direct forbidden band gap of 1.4 eV, an optical absorption coefficient of  $1 \times 10^5 \text{ cm}^{-1}$  at 1.9 eV, electrical resistivity of 84–9.6  $\Omega \text{ cm}$ , and p-type conductivity, also support potential application as a solar absorber in photovoltaic devices.

**Acknowledgment.** The authors acknowledge George Braybrook for collection of SEM images and EDX data, Sergi Matveev for collection of WDX data, and the National Institute for Nanotechnology for access to SEM and XRD instruments. Funding was provided by an NSERC-Natural Resources Canada Greenhouse Gas Mitigation Program grant (GHGP J 269903) awarded to J.A.H. N.J.G. thanks NSERC and Alberta Ingenuity for graduate studentships.

**Supporting Information Available:** Plots of  $(\alpha h\nu)^{1/n}$  against  $h\nu$  with  $1/n = 2, 2/3, 1/2,$  and  $1/3$ . This material is available free of charge via the Internet at <http://pubs.acs.org>.

CM061453R